International Journal of Mathematics and Physical Sciences Research ISSN 2348-5736 (Online)
Vol. 10, Issue 2, pp: (80-93), Month: October 2022 - March 2023, Available at: www.researchpublish.com

Unsteady Heat and Mass Transfer MHD Flow of Nano-Fluids with Buoyancy and Variable Thermal Conductivity

Akindele M. Okedoye[1,2], Azeez A. Waheed[3], Olufemi. A. Akinyemi[2]

[1]Department of Mathematics, Covenant University, Ota, Ogun State, Nigeria

[2]Department of Mathematics, Federal University of Petroleum Resources, Effurun, Nigeria

[3]Department of Mathematics, Lead City University, Ibadan, Oyo State Nigeria

DOI: https://doi.org/10.5281/zenodo.7669943

Published Date: 23-February-2023

Abstract: **Scientists and engineers have conducted a considerable lot of experimental and theoretical study to increase the productivity of industrial operations. Experimental evidence from engineers and scientists shows that heat transfer is necessary for excellent multi scale production naturally, continuous phase liquids are used to achieve thermal characteristics. However, due to the limitations of heat transmission, their significance is constrained. We present a mathematical model for unsteady heat and mass transfer in MHD flow of Nano-fluid with buoyancy and variable thermal conductivity. Using self-similar variables, the coupled non-linear system of equations governing the boundary-layer flows of Nano-fluids were converted into a two-point boundary value problem. The dsolve command with the numeric option on a real-valued two-point boundary value problem (BVP) is used to finds a numerical solution for our system of equations. Computation is performed in both hardware precision and arbitrary precision. The output of the computation is plotted using the ode plot generator odeplot and displayed using Maple plot display, and wall rate transfer is extracted. From the result, increase in thermal buoyancy, unsteadiness parameter and suction parameter are seen to increase velocity distributions. Temperature boundary layer is enhanced with increase in unsteadiness parameter, Brownian motion parameter and Eckert number while radiation, thermophoretic diffusion parameter, reactivity parameter, thermal conductivity and suction enhances species concentration.**

Keywords: **Unsteady, Heat and Mass Transfer, Nano-Fluids, Buoyance, Variable Thermal Conduction, thermo-gravitational, Navier Stokes, magneto hydrodynamics.**

I. INTRODUCTION

Recently, scientists and engineers have conducted a considerable lot of experimental and theoretical study to increase the productivity of industrial operations. Experimental evidence from engineers and scientists shows that heat transfer is necessary for excellent multi scale production naturally, continuous phase liquids are used to achieve thermal characteristics. However, due to the limitations of heat transmission, their significance is constrained. In order to achieve the predicted results, researchers believed that improved heat transport phenomenon should be used. They discovered that a continuous phase liquid's thermal capacity can be improved through intensifying its thermal conductance in order to achieve such goals. This introduces the idea of adding materials to continuous phase liquid to create a superior transport medium. Due to their unique chemical and physical properties, these nanoparticles are highly intriguing. It is believed that adding nanoparticles improves the thermal properties of continuous phase liquid. In light of this, excited researchers have begun to focus on convective heat transport through Nano-material. Nano materials were first introduced by Choi [1]. He defined such idea of nanomaterials in a continuous phase liquid. He used experiments to demonstrate that the thermal properties of continuous phase liquids were improved by the use of such nanoparticles. By providing a model to assess the thermal properties of

continuous phase liquids, Buongiorno [2] presented research on nano-materials. He predicted that the small size and low volume percentage of supplemental nanoelements would be the cause of the continuous phase liquid's increased conductivity. In numerous industries, such as transportation, micro scale items, cancer therapy, power generation, and chemical and metallurgical devices, nanotechnology is crucial. Pandey and Kumar [3] have studied the heat transfer in the flow of a stretched cylinder made of copper-water nanomaterial. Recent years have seen a thorough analysis of Newtonian liquids developed using Navier-Stokes expressions. This is mostly due to the fact that these liquids are simple, making their solution convenient [4, 5]. However, Newtonian liquids that are linearly related to shear stress and strain rate are insufficient for their intended uses. These liquids don't exhibit many of the phenomena that are observed for liquids in technological and industrial applications.

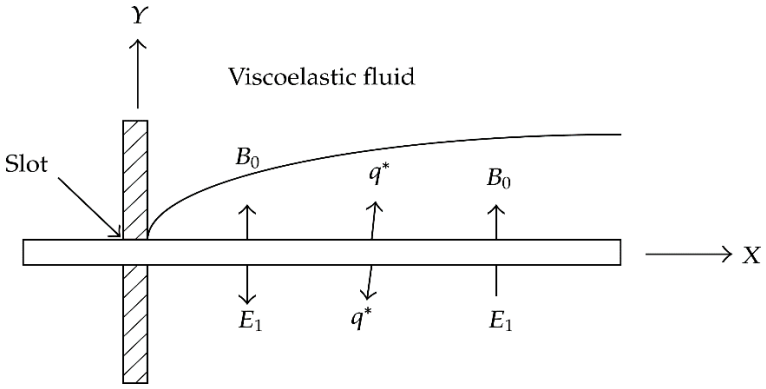

Figure 1: Model Configuration

Soap, greases, blood, elastomers, suspensions, clay coating, and various emulsions are a few examples of multifarious liquids that are important due to their various industrial applications. However, Navier-Stokes expressions fall short when it comes to describing these so-called non-Newtonian liquids. These liquids are created via a non-linear relationship between shear stress and strain rate. Since non-Newtonian liquids make a considerable contribution to engineering and industry, understanding their flow characteristics is crucial. Due to widespread applications in several fields of geophysics, bio rheology, petroleum, and chemical industries, this relevance is stimulated. These applications have made the study of non-Newtonian liquids and the investigation of their properties an increasingly interesting topic of modern research.

Muhammad et al. [6, 7] investigated magneto hydrodynamics (MHD) radiated second order slip of nanomaterial on a curved surface with thermal radiation, viscous dissipation, mixed convection, chemical reaction, and activation energy. Because matter behaves and has different properties at the Nano-scale compared to regular macroscopic dimensions, Nano-biotechnology is a brand-new, interdisciplinary science with ground-breaking perspectives. A new method of creating and obtaining materials, structures, and gadgets with significantly enhanced or entirely new qualities and capabilities is known as nanotechnology. Paolo [8]. Utilizing features and chemical-physical processes that appear at such scales, nanotechnologies govern and alter matter at the Nano-metric level. In recent years, many empirical technologies, including those related to ceramics, metallurgy, photography, heterogeneous catalysis, resins and polymers, and special compounds for pneumatic tires, have undergone complete or partial understanding and reconsideration in relation to their Nano-scale structures and mechanisms Paolo [9]

The needs of industry or technology can be satisfied with a new generation of fluid with good thermal performance. A hybrid Nano-fluid combines two different kinds of nanoparticles with a base fluid (for example, water, ethylene glycol, or a combination of ethylene glycol and water) (i.e. metal oxides, metals, carbon materials). The stability of the resulting hybrid Nano-fluid might be maintained, according to Suresh et al. [10], by adding the least number of copper nanoparticles possible in a quantity that is appropriate to the alumina matrix. Though its thermal conductivity is less than that of copper nanoparticles, alumina nanoparticles exhibit good chemical inactivity and stability. Using an alumina-water Nano-fluid, Mansoury et al. [11] examined the heat transfer capabilities of parallel flow heat exchangers. They discovered that, when compared to two shell-and-tube heat exchangers and a plate heat exchanger, the double-pipe heat exchanger exhibited the greatest heat transfer enhancement. Ma et al. [12] used numerical analysis to study the natural convection heat transport of CuO-water Nano-fluid in a U-shaped enclosure with a baffle. They demonstrated that an increase in the volume fraction of nanoparticles caused an increase in the average Nusselt number. Additionally, these researchers have reviewed the uses, creation, and thermo-physical characteristics of both normal and hybrid Nano-fluids (see Jana et al. [13], Sarkar et al. [14], Sidik et al. [15], Akilu et al. [16], Babu et al. [17], Sundar et al. [18], Leong et al. [19], Huminic and Huminic [20] and Sajid

and Ali [21]). Researchers are also drawn to the study of hybrid Nano-fluids made of Nano-encapsulated phase transition materials (see Ghalambaz et al. [22–24] and Hajjar et al. [25]). Due to its many engineering applications in heat exchangers, HVAC (heating, ventilation, and air conditioning), and building insulation, the heat transfer mechanism associated to a cavity has also generated interest. The numerical simulation for hybrid Cu-Al2O3/water Nano-fluid flow and heat transfer from a cavity was carried out by Chamkha et al. [26]. Using the local thermal none-equilibrium (LTNE) model, Ghalambaz et al. [27] examined Ag-MgO hybrid Nano-fluid flow and heat transport within a porous square cavity. They discovered that the flow strength and heat transfer rate were decreased when hybrid nanoparticles were used. Sheremet et al. [28] examined the thermo-gravitational convection of a hybrid Al2O3-SiO2/water Nano-fluid in a porous chamber.

Despite the contributions of the above authours, the unsteady heat and mass transfer in MHD flow of Nano-fluid with buoyancy and variable thermal conductivity has not been adequately reported. Hence in this report, we have considered the aforementioned with particular references to velocity, thermal and chemical species slips.

II. MATHEMATICAL MODELLING

The first step in creating a mathematical theory of boundary layers is to demonstrate the existence of a limiting form of the equations of motion that differs from the one created by setting $\upsilon = 0$ in the first place as the Reynolds number R or the kinematic viscosity tend to infinity or zero, respectively. It is hence reasonable to predict that a solution of these limiting equations will roughly reflect the flow in a laminar boundary layer for which R is big but not infinite.

The full equation of motion for a two-dimensional flow are:

$$\frac{\partial u}{\partial x} + \frac{\partial v}{\partial y} = 0 \tag{1}$$

$$\begin{aligned} \frac{\partial u}{\partial t} + u\frac{\partial u}{\partial x} + v\frac{\partial u}{\partial y} = & -\frac{1}{\rho_{n_f}}\frac{\partial p}{\partial x} + \upsilon_{n_f}\frac{\partial^2 u}{\partial y^2} + \frac{\alpha_{n_f}}{\rho_{n_f}}\tau - \frac{\sigma\mu B_o^2(x)}{\rho_{n_f}k}(u - U) \\ & \mp \frac{g}{\rho_{n_f}}\left(\frac{K_1}{\upsilon}\right)|\hat{u}|(u - U) + \frac{g}{\rho_{n_f}}\left(\beta_\tau(T - T_\infty) + \beta_c(C - C_\infty)\right) \end{aligned} \tag{2}$$

Energy transfer equation becomes

$$\begin{aligned} \rho_{n_f}c_p\left(\frac{\partial T}{\partial t} + u\frac{\partial T}{\partial x} + v\frac{\partial T}{\partial y}\right) = & \frac{\partial}{\partial y}\left(k_T\frac{\partial T}{\partial y}\right) \\ & + N_{n_f}\left\{D_m\frac{\partial T}{\partial y}\frac{\partial C}{\partial y} + \frac{D_T}{T_\infty}\left(\frac{\partial T}{\partial y}\right)^2 + \left(\frac{\partial u}{\partial y}\right)^2\right\} - \frac{\partial q_r}{\partial y} + q''' \end{aligned} \tag{3}$$

Mass transfer (species) equation becomes

$$\frac{\partial C}{\partial t} + u\frac{\partial C}{\partial x} + v\frac{\partial C}{\partial y} = \frac{D_m}{\rho_{n_f}}\frac{\partial^2 C}{\partial y^2} + R_A - \frac{1}{\rho_{n_f}}\frac{\partial}{\partial y}\left((C - C_\infty)V_T\right) \tag{4}$$

The viscoelastic function is given by

$$\tau = \frac{\partial u}{\partial x}\frac{\partial^2 u}{\partial y^2} + u\frac{\partial^3 u}{\partial y^2 \partial x} - \frac{\partial u}{\partial y}\frac{\partial^2 u}{\partial y \partial x} + v\frac{\partial^3 u}{\partial y^3} \tag{5}$$

It is assumed that the radiation heat flux is to be presented in the form of an unidirectional flux in the y direction. Using the Roseland approximation for radioactive heat transfer and the Roseland approximation for diffusion, the expression for the radioactive heat flux q_r can be given as

$$q_r = \left(\frac{-4\sigma}{3k_s}\right)\left(\frac{\partial T^4}{\partial y}\right) \tag{6}$$

Here in Eq.(7), the parameters σ and k_s represent the Stefan Boltzmann constant and the Roseland mean absorption coefficient, respectively.

Now on assuming that the temperature differences within the fluid flow are sufficiently small, T^4 in Eq.(7) can be expressed

as a linear function of T_∞ ' using the Taylor series expansion. The Taylor series expansion of T^4about T_∞ , after neglecting the higher order terms, takes the form

$$T^4 \cong 4T_\infty^3 T - 3T_\infty^4 \tag{7}$$

We employed chemical reaction of Arrhenius type of the *1st* order irreversible reaction given by,

$$R_A = k_r^2(T\ -\ T\infty)^r \exp\left(-\frac{E_a}{R_G T}\right)(C\ -\ C_\infty) \tag{8}$$

Where k_r is the reactivity of chemical reaction defined by frequency of collision ω and orientation factor p as $k_r = k_r(\omega, p) = \omega p$, R_G is the universal gas constant.

In the same analysis, non-uniform heat source/sink (q''') and thermo-phoretic velocity (V_T) are given by

$$\begin{aligned} q''' &= \left(\frac{\kappa u_w(x)}{x\nu}\right)\left[\frac{A^*(T_w - T_\infty)}{bx}(u-U) + B^*(T-T_\infty)\right] \\ V_T &= \frac{k'\nu}{\tau}\frac{\partial T}{\partial y} \end{aligned} \tag{9}$$

Following Arunachalam and Rajappa [29] and Chain [30] the thermal conductivity K_T is taken as

$$k_T = k\frac{T}{T_\infty} \tag{10}$$

The thermal boundary conditions depend on the type of heating process under consideration. In the present investigation, the heat transfer analysis has been carried out for two different heating processes namely VWT and VHF cases.

$$q_r = \left(\frac{-16\sigma T_\infty^3}{3k_s}\right)\left(\frac{\partial T}{\partial y}\right) \tag{11}$$

Far away from the plate, $u \to U(t), T \to T_\infty, C - C_\infty$

$$\frac{\partial U}{\partial t} + \frac{\sigma\mu B_o^2(x)}{\rho_{n_f} k}U \mp \frac{g}{\rho_{n_f}}\left(\frac{K_1}{\upsilon}\right)|\hat{u}|(U)\ =\ -\frac{1}{\rho_{n_f}}\frac{\partial p}{\partial x} \tag{12}$$

Using equations (6) and (9) – (13), equations (2) – (5) becomes

$$\begin{aligned} \frac{\partial u}{\partial t} + u\frac{\partial u}{\partial x} + v\frac{\partial u}{\partial y} &= \upsilon_{n_f}\frac{\partial^2 u}{\partial y^2} - \frac{\sigma\mu B_o^2(x)}{\rho_{n_f} k}(u-U) + \frac{\alpha_{n_f}}{\rho_{n_f}}\left(\frac{\partial u}{\partial x}\frac{\partial^2 u}{\partial y^2} + u\frac{\partial^3 u}{\partial y^2 \partial x} - \frac{\partial u}{\partial y}\frac{\partial^2 u}{\partial y \partial x} + v\frac{\partial^3 u}{\partial y^3}\right) \\ &\quad -\frac{1}{\rho}\frac{\partial P}{\partial x} \mp \frac{g}{\rho_{n_f}}\left(\frac{k_r}{\upsilon}\right)|\hat{u}|(u-U) + \frac{g}{\rho_{n_f}}\left(\beta_\tau(T-T_\infty) + \beta_c(C-C_\infty)\right) \end{aligned} \tag{13}$$

$$\begin{aligned} \rho_{n_f} c_p\left(\frac{\partial T}{\partial t} + u\frac{\partial T}{\partial x} + v\frac{\partial T}{\partial y}\right) &= \frac{\partial}{\partial y}\left(k_T\frac{\partial T}{\partial y}\right) + N_{n_f}\left\{D_m\frac{\partial T}{\partial y}\frac{\partial C}{\partial y} + \frac{D_T}{T_\infty}\left(\frac{\partial T}{\partial y}\right)^2 + \left(\frac{\partial u}{\partial y}\right)^2\right\} \\ &\quad + \left(\frac{16\sigma T_\infty^3}{3k_s}\right)\frac{\partial^2 T}{\partial y^2} + \left(\frac{\kappa u_w(x)}{x\nu}\right)\left[\frac{A^*(T_w - T_\infty)}{bx}(u-U) + B^*(T-T_\infty)\right] \end{aligned} \tag{14}$$

$$\frac{\partial C}{\partial t} + u\frac{\partial C}{\partial x} + v\frac{\partial C}{\partial y} = \frac{D_m}{\rho_{n_f}}\frac{\partial^2 C}{\partial y^2} + k_r^2(T\ -\ T\infty)^r \exp\left(-\frac{E_a}{R_G T}\right)(C\ -\ C_\infty) - \frac{k'\nu}{\tau\rho_{n_f}}\frac{\partial}{\partial y}\left((C-C_\infty)\frac{\partial T}{\partial y}\right) \tag{15}$$

$A^*, B^* > 0\ and\ A^* = (T_w - T_\infty),\ B^* = (C_w\ -\ C_\infty).$

The appropriate initial and boundary conditions relevant to the problem are

$$\begin{aligned} &t \le 0: u\ =\ ax, \quad T\ =\ T_w, C\ =\ C_w\ \forall y \\ &t > 0: \left\{\begin{array}{c} u\ =\ U_0(B)ax, v = v_w, -k\frac{\partial T}{\partial y} =\ h(T_w - T), \\ -D_B C_y\ =h_2(T_w - T), \end{array}\right\}\ y\ =\ 0 \\ &u\ \to\ 0, u_y \to 0, T\ \to\ T_\infty, C\ \to\ C_\infty\ as\ y\ \to\ \infty \end{aligned} \tag{16}$$

The stream velocity is given by

$$U(t) = \frac{ax}{1-\lambda t} \tag{17}$$

while at time $y = 0$, the suction/blowing is a function free stream given as

$$v(t,0) = v_w(t) \tag{18}$$

III. METHOD OF SOLUTION

The governing system of equations described by equations (13)-(15) subject to (16) is transformed into system of ordinary differential equations using the self-similar variables which satisfy the stream function defined as follows:

$$\begin{gathered}\psi(x,y,t) = \left(\frac{a\nu}{1-\lambda t}\right)^{1/2} x f(\eta), \eta(y,t) = \left(\frac{a}{1-\lambda t}\right)^{1/2} y, \\ \theta(\eta) = \frac{T-T_\infty}{T_w - T_\infty}, \phi(\eta) = \frac{C-C_\infty}{C_w - C_\infty}\end{gathered} \tag{19}$$

where η is similarity variable and ψ is stream function defined as $u = \partial\psi/\partial y$ and $v = -\partial\psi/\partial x$ thus we have

$$u = \frac{ax}{1-\lambda t} f'(\eta), \qquad v = -\left(\frac{a\nu}{1-\lambda t}\right)^{1/2} f(\eta) \tag{20}$$

Using (22) and (23), we have

$$\begin{gathered}f'''(\eta) + f(\eta)f''(\eta) - \left(f'(\eta)\right)^2 + A\left(1 - f'(\eta) - \frac{1}{2}\eta f''(\eta)\right) - (Ha + Fs)(f'(\eta) - 1) \\ +\beta\left(2f'(\eta)f'''(\eta) - f''(\eta)^2 - f(\eta)f^{iv}(\eta)\right) + Grt\ \theta(\eta) + Grc\ \theta(\eta) = 0\end{gathered} \tag{21}$$

$$\begin{gathered}\left(1 + \frac{4}{3}R + \alpha\theta(\eta)\right)\theta''(\eta) - Pr\left(A\frac{1}{2}\eta - f(\eta)\right)\theta'^{(\eta)} + Nb\theta'(\eta)\phi'(\eta) \\ +(Nt + \alpha)\theta'(\eta)^2 + Ec\theta''(\eta)^2 + \Pr\left(A^*(f'(\eta) - 1) + B^*\vartheta(\eta)\right) = 0\end{gathered} \tag{22}$$

$$\phi''(\eta) - Sc\left(A\frac{1}{2}\eta - f(\eta)\right)\phi'(\eta) - \Omega\left(\phi'(\eta)\theta'(\eta) + \phi(\eta)\theta''(\eta)\right) + Sc\delta\theta(\eta)^r e^{\frac{\theta(\eta)}{1+\epsilon\theta(\eta)}}\phi(\eta) = 0 \tag{23}$$

The corresponding initial-boundary conditions becomes

$$\begin{gathered}f'(0) = 1 - M_s, f(0) = f_w, \theta'(0) = Bi(\theta(0) - 1), \phi'(0) = \gamma(\phi(0) - 1) \\ f'(\infty) \to 0, f''(\infty) \to 0, \theta(\infty) \to 0, \phi(\infty) \to 0\end{gathered} \tag{24}$$

where

$$Bi = \frac{h_1}{k}\left(\frac{\nu(1-\lambda t)}{a}\right)^{1/2}, \gamma = \frac{h_2}{D_B}\left(\frac{\nu(1-\lambda t)}{a}\right)^{1/2}, M_s = \frac{\sigma B_0^2 L}{a\rho_{nf}}, f_w = v_w\left(\frac{(1-\lambda t)}{\nu a}\right)^{1/2}$$

$$Ec = \frac{krax^2\rho_{nf}}{(T_w - T_\infty)k}, Ha = \frac{\sigma\mu_{nf}B_0^2}{a\rho_{nf}}, \beta = \frac{\alpha_{nf}}{\mu_{nf}}\frac{a}{(1-\lambda t)},$$

$$Grt = g\beta_t\frac{(1-\lambda t)^2}{a^2 x}(T_w - T_\infty), Grc = g\beta_t\frac{(1-\lambda t)^2}{a^2 x}(C_w - C_\infty), \frac{g}{\rho_{n_f}}\left(\frac{K_1}{\upsilon}\right)\frac{L}{U}|\hat{u}| = Fs,$$

$$Pr = \frac{\mu_{nf}c_{p_{nf}}}{k}, \frac{\mu_{nf}}{D_B} = Sc, k_r\frac{(T_w - T_\infty)^r D_T}{\rho_{n_f}T_\infty e^{\left(\frac{1}{\epsilon}\right)}} = \delta, \Omega = \frac{(T_w - T_\infty)}{D_B}\frac{k_1\nu_{nf}}{\tau\rho_{nf}}, R = \frac{4\sigma T_\infty^2}{k_s k},$$

$$A = \frac{\lambda}{a}, \frac{c_p(T_w - T_\infty)D_T}{\rho T_\infty k} = Nt, \frac{c_p(C_w - C_\infty)D_m}{\rho T_\infty k} = N_b, M_s = \frac{\sigma\mu_f B_0^2}{a\rho_f/L}$$

IV. RESULTS AND DISCUSSIONS

In other to analyse the solution of the system of equations (21)-(23) subject to (24), we use differential solver, dsolve is maple release 2021 with inbuilt numerical generator madrich with $Ec = 0.4, Grc = 1.5, Grt = 2, Ha = 1, Le = 1.0, Nb = 0.5, Nt = 0.2, Pr = 1.0, \beta = 0.1, \delta = 0.5, \gamma = 0.2, \lambda = 0.3, n = 1.2$ as prescribe parameters. The dsolve command with the numeric option on a real-valued two-point boundary value problem (BVP), finds a numerical solution for our system of equations. The bvp under consideration is automatically detected by dsolve submethod which uses midrich algorithm is used as solver. The choice of madrich is hinged on its ability to use Richardson extrapolation enhancement or deferred correction enhancement. Computation is performed in both hardware precision and arbitrary precision, by the setting of Digits to 20. This is good enough to maintain both precisions either when Digits is smaller than the hardware precision for the machine or when Digits is larger. The computations were done by a program which uses a symbolic and computational computer language MAPLE. A step size of $\Delta\eta = 0.001$ was selected to be satisfactory for a convergence criterion of 10^{-7} in nearly all cases. The value of η_∞ was found to each iteration loop by the assignment statement $\eta_\infty = \eta_\infty + \Delta\eta$. The maximum value of η_∞, to each group of parameters is determined when the values of unknown boundary conditions at $\eta = 0$ not change to successful loop with error less than 10^{-7}.

The output of the computation is plotted using the ode plot generator odeplot and displayed using Maple plot display, and wall rate transfer is extracted. The graphical results and wall rate transfer are presented below in Figure (2) – (25) and Table (1).

A. Velocity distribution

Velocity distribution was examined under the influences of thermal buoyancy Gtt, unsteadiness parameter A, viscoelastic parameter β, Hartmann number Ha, velocity slip factor Ms , suction velocity f_w, variable thermal conductivity factor α, and radiation parameter R Figure 2 demonstrates how increasing thermal Gasohof number parameter result in higher velocity profiles. With increase in Grashof number, there is emergence of maximum velocity in the body of the fluid close to the surface. Close to 3 units away from the surface, we notice a point of mixed convection where the velocity properties were reversed. From Figure 3, the effect of unsteadiness parameter was displayed. The Figure shows that increase in unsteadiness parameter increases the bulk velocity of the flow. From the Figure 4 and 5 we observed that increase in both Hartmann number and velocity slip factor decline while at about 2 units away from the surface, the flow velocity property increases with increase in Hartmann number due to mixed convective force on the flow. From Figures 5, 8 and 9, we observed that velocity increases with an increase in suction velocity, variable thermal conductivity and radiation parameter. In those scenarios, maximum velocity was discovered to exist close to the surface for lower values of suction, velocity, variable thermal conductivity and radiation parameter. The effect of viscoelastic parameter was discovered to enhances the velocity as shown in Figure 7

B. Temperature distribution

The temperature distribution of the flow under consideration was discussed under radiation parameter R, variable thermal conductivity parameter, unsteadiness parameter, Brownian motion, thermophoretic parameter, Eckert number and convective surface heat transfer. Unsteadiness parameter, Brownian motion parameter and Eckert number we discovered to enhance the temperature distribution of the flow field as displayed in Figures 10, 14 and 15. While in Figures 12, 13, 16 and 17 the radiation parameter, variable thermal conductivity suction velocity and Hartmann number impose adverse effect on the temperature distribution with a decrease in the temperature boundary layer as the parameters increases. The effect of convective surface heat transfer is displayed in Figure 11. From this figure, we discovered that the bulk temperature of the flow field increases with heat moving from the solid surface to the fluid ($Bi < 0$) while it decreases when he at moves from the fluid to the solid surface ($Bi > 0$)

TABLE 1: WALL TRANSFER RATE FOR VARIOUS VALUES OF PARAMETERS

Parameters	$f''(\eta)$	ϕ'	θ'	Parameters	$f''(\eta)$	ϕ'	θ'
$A = 0.0$	0.1768	-0.1927	0.2071	$Ec = 1.0$	0.2451	-0.1929	0.2134
$A = 0.2$	0.2868	-0.1941	0.2627	$Ec = 2.0$	0.2737	-0.1933	0.2316
$A = 0.6$	0.4421	-0.1955	0.3435	$Ec = 3.0$	0.3094	-0.1939	0.2544
$A = 1.2$	0.7088	-0.1971	0.4881	$Ec = 4.0$	0.3562	-0.1945	0.2843
$Fs = 0.0$	0.2865	-0.1936	0.2435	$B* = 0.1$	0.2737	-0.1933	0.2316

$Fs = 0.2$	0.2737	-0.1933	0.2316	$B* = 0.5$	-0.3008	-0.1517	-0.1441
$Fs = 0.4$	0.2641	-0.1931	0.2214	$B* = 1.0$	-0.2552	-0.1569	-0.1087
$Fs = 2.0$	0.2454	-0.1916	0.1736	$B* = 1.5$	-0.4250	-0.1541	-0.2348
$\beta = 0.1$	0.2737	-0.1933	0.2316	$\Omega = 0.1$	0.2737	-0.1934	0.2316
$\beta = 0.3$	0.3209	-0.1933	0.2305	$\Omega = 0.3$	0.2741	-0.1916	0.2314
$\beta = 0.8$	0.4035	-0.1933	0.2311	$\Omega = 0.8$	0.2744	-0.1903	0.2313
$\beta = 1.4$	0.6195	-0.1935	0.2397	$\Omega = 1.4$	0.2748	-0.1887	0.2312
$Grt = 0.0$	0.0649	-0.1995	1.3743	$\delta = -1.0$	0.2748	-0.1908	0.2316
$Grt = 0.5$	0.3326	-0.1962	0.3989	$\delta = -0.5$	0.2770	-0.1873	0.2319
$Grt = 1.5$	0.6811	-0.1935	0.2335	$\delta = -0.2$	0.2836	-0.1809	0.2334
$Grt = 2.5$	1.0995	-0.1943	0.2708	$\delta = 0.0$	0.3427	-0.1434	0.2522
$Grc = 0.3$	0.3976	-0.1952	0.3201	$\gamma = 1.2$	0.2697	-3.6672	0.2078
$Grc = 0.8$	-0.2497	-0.1506	-0.1492	$\gamma = 0.8$	0.2696	-2.8429	0.2134
$Grc = 1.3$	-0.1319	-0.1511	-0.1505	$\gamma = 0.4$	0.2710	-1.4744	0.2228
$Grc = 2.0$	0.0831	-0.1513	-0.1637	$\gamma = 0.2$	0.2730	-0.4601	0.2298
$Ha = 0.1$	0.5384	-0.1962	0.3967	$f_w = 0.0$	0.4144	-0.1952	0.3256
$Ha = 0.5$	0.3976	-0.1952	0.3201	$f_w = 0.2$	0.1260	-0.1902	0.1376
$Ha = 1.5$	0.2737	-0.1933	0.2316	$f_w = 0.4$	-0.0202	-0.1851	0.0484
$Ha = 2.5$	0.2460	-0.1922	0.1919	$f_w = 1.4$	-0.3087	-0.1647	-0.1157
$R = 1.0$	0.2737	-0.1933	0.2316	$Bi = -0.6$	-0.1107	-0.1770	0.0687
$R = 2.0$	-0.0108	-0.1846	0.0462	$Bi = -0.2$	-0.1447	-0.1732	0.0460
$R = 3.0$	-0.1006	-0.1782	-0.0136	$Bi = 0.2$	0.2737	-0.1933	0.2316
$R = 4.0$	-0.1550	-0.1722	-0.0508	$Bi = 0.8$	-0.0343	-0.1831	0.1131
$\alpha = 0.1$	0.4035	-0.1951	0.3185	$r = 1.0$	0.2779	-0.1862	0.2320
$\alpha = 0.3$	0.2737	-0.1933	0.2316	$r = 2.0$	0.2750	-0.1904	0.2316
$\alpha = 1.5$	0.0774	-0.1884	0.1004	$r = 3.0$	0.2737	-0.1933	0.2316
$\alpha = 3.0$	0.0072	-0.1853	0.0536	$r = 4.0$	0.2733	-0.1954	0.2318
$Nb = 0.2$	0.2753	-0.1934	0.2327	$Nt = 0.2$	0.1757	-0.1915	0.1701
$Nb = 0.4$	0.2737	-0.1933	0.2316	$Nt = 0.4$	0.2737	-0.1933	0.2316
$Nb = 0.8$	0.2717	-0.1933	0.2303	$Nt = 0.8$	0.6503	-0.1969	0.4661
$Nb = 1.2$	0.2657	-0.1932	0.2263	$Nt = 1.2$	1.0532	-0.1984	0.7148
$Sc = 0.60$	0.2737	-0.1933	0.2316	$Pr = 0.01$	-0.1778	-0.1691	-0.0670
$Sc = 0.78$	0.2735	-0.1941	0.2317	$Pr = 0.71$	0.1539	-0.1908	0.1527
$Sc = 1.20$	0.2733	-0.1953	0.2318	$Pr = 4.00$	0.2559	-0.1930	0.2198
$Sc = 2.60$	0.2733	-0.1968	0.2321	$Pr = 7.00$	0.3344	-0.1943	0.2726

C. Concentration distribution

The chemical species concentration of the flow under consideration was analysed under the influence of radiation parameter R, Thermophoretic Diffusion Coefficient, Chemical reaction parameter, concentration slip factor and reaction order, variable thermal conductivity parameter, and suction velocity. We discovered that as the unsteadiness parameter increases, the species concentration boundary layer declines so also an increase in both concentration slip factor and reaction order as displayed in Figures 18, 21 and 23 respectively. Figure 19 reveals that as radiation parameter increases it is equally increase the bulky of concentration. The effect of Thermophoretic Diffusion Coefficient Ω on the concentration field shown in Figure 20. From this Figure we see that the effect display various values of Thermophoretic Diffusion Coefficient as the value increases it increases the bulk of concentration profile. Figure 22 shows the effect of reactivity parameter on concentration profiles. It is clear from this Figure that concentration decreases for destructive chemical reactions ($\delta > 0$) and increases for generative chemical reactions ($\delta < 0$) Figure 24 and 25 shows the effect of variable thermal conductivity parameter and suction velocity parameter on concentration profiles respectively. From these figures, we discovered that increase in these parameters enhances the species boundary layer.

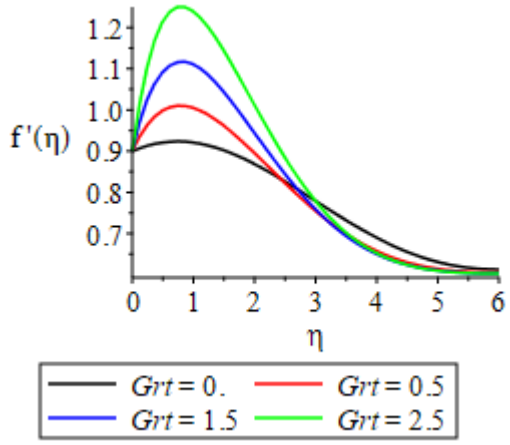

Figure 2: Velocity Distributions for various of valuesThermal Grashoof number

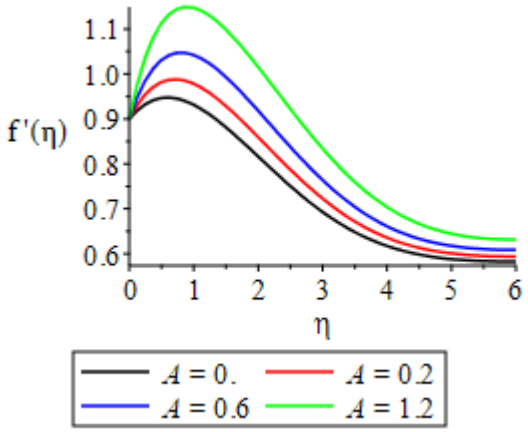

Figure 3: Velocity Distributions for various values of unsteadiness parameter

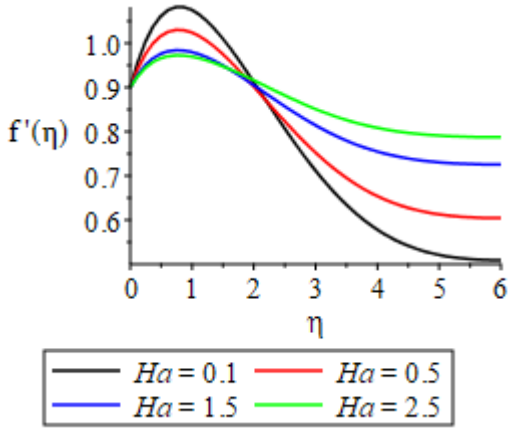

Figure 4: Velocity Distributions for various values values of Hartmann number.

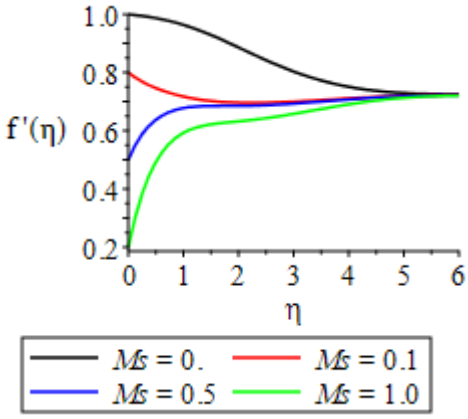

Figure 5: Velocity Distributions for various values of velocity slip

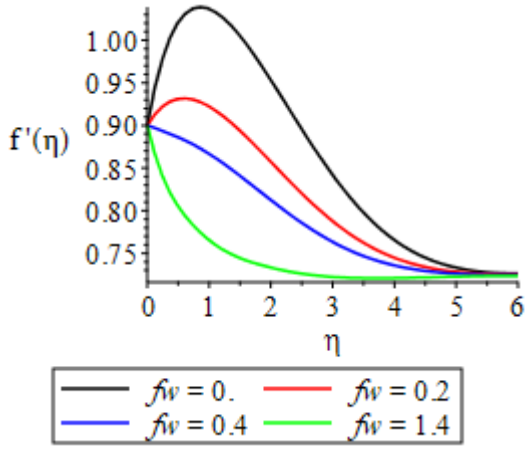

Figure 6: Velocity Distributions for various values values of suction parameter

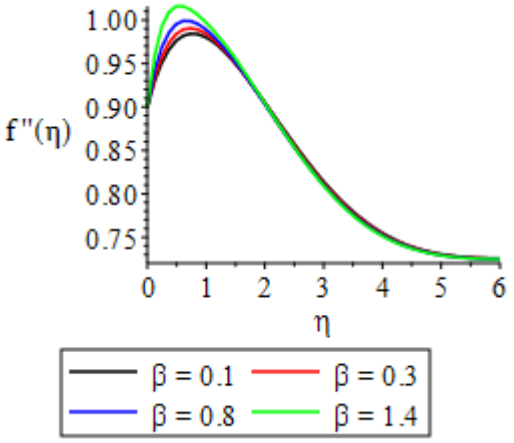

Figure 7: Velocity Distributions for various values values of viscoelastic parameter

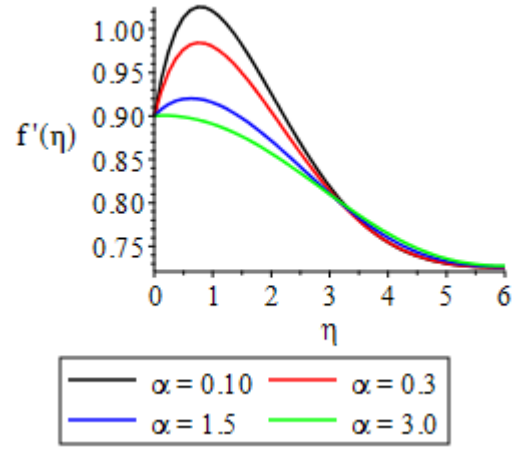

Figure 8: Velocity Distributions for various values values of variable thermal conductivity.

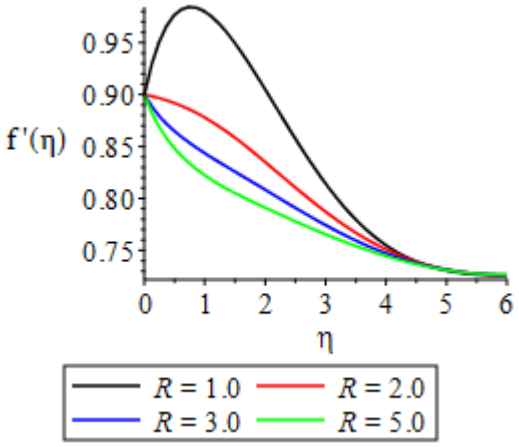

Figure 9 : Velocity Distributions for various values values of radiation parameter

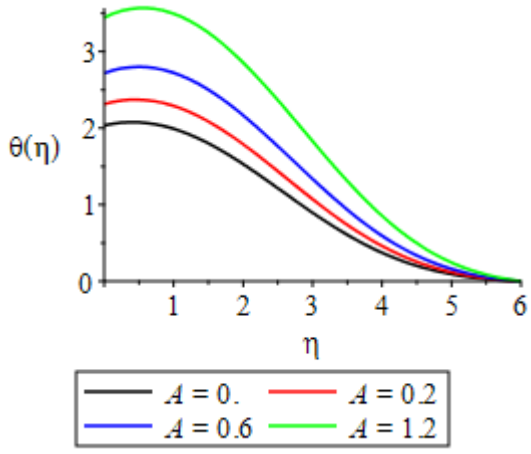

Figure 10: Temperature Distributions for various values of unsteadiness parameter

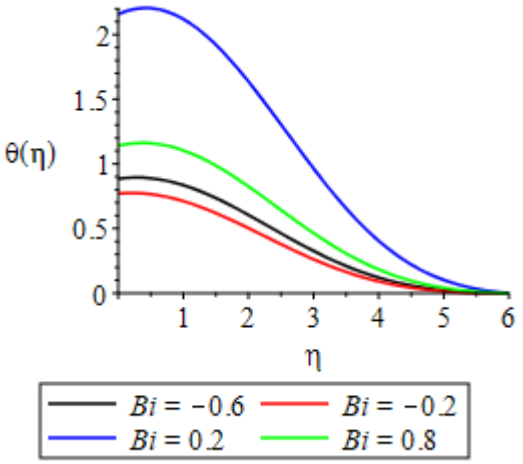

Figure 11: Effect of Convective heat transfer on Temperature Distributions

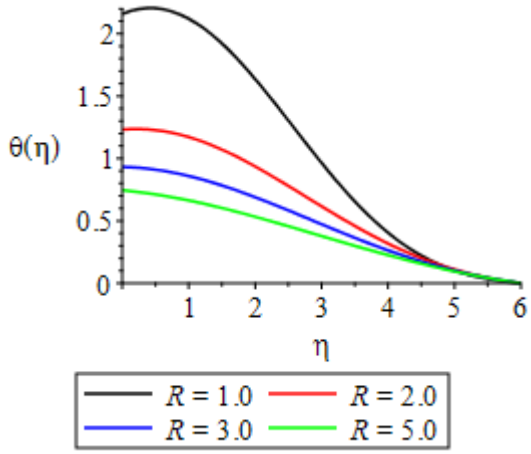

Figure 12: Effect of radiation parameter on Temperature Distributions

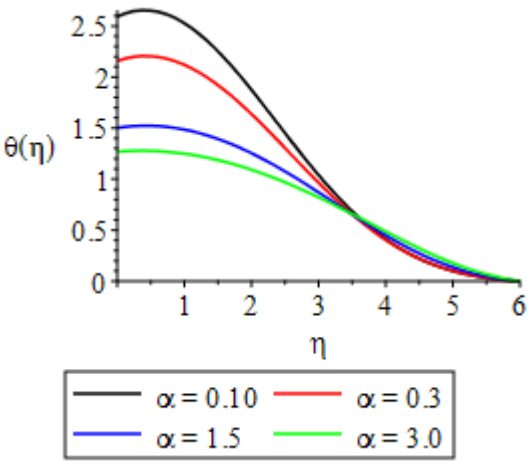

Figure 13: Effect of variable thermal conductivity on Temperature Distributions

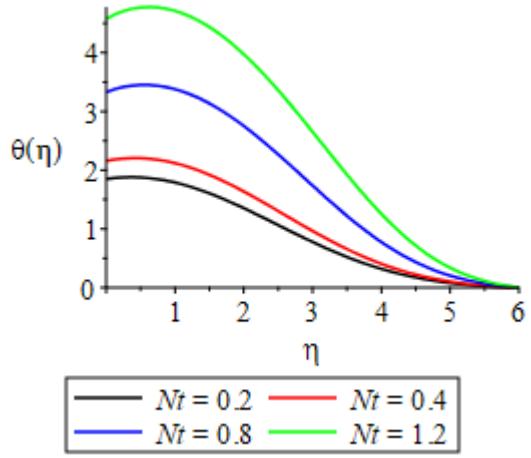

Figure 14: Effect of Nt on Temperature Distributions

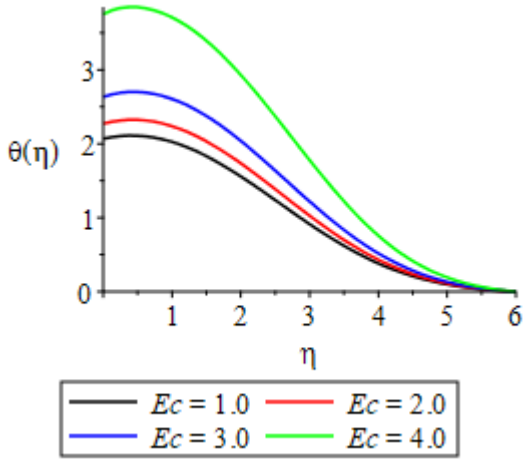

Figure 15: Effect of Eckert number on Temperature Distributions

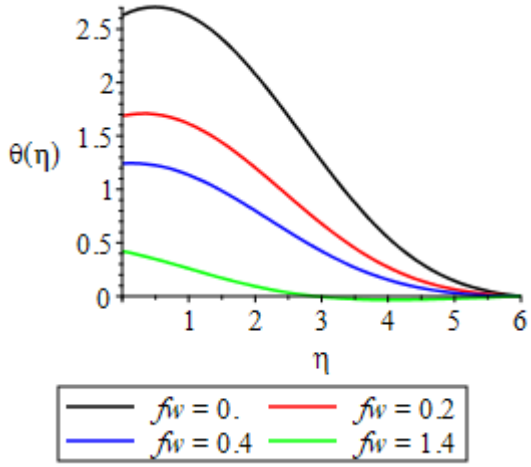

Figure 16: Temperature Distributions for various values of suction parameter

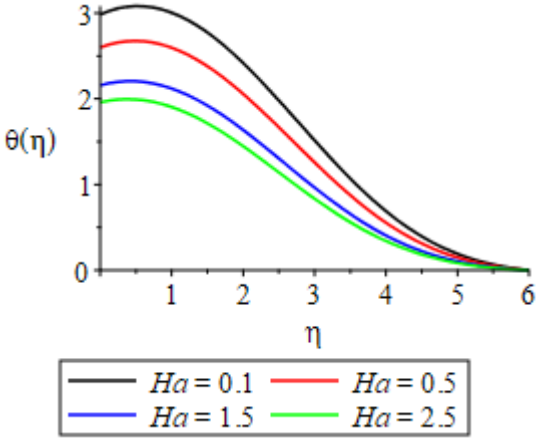

Figure 17: Temperature Distributions for various values of Hartmann number

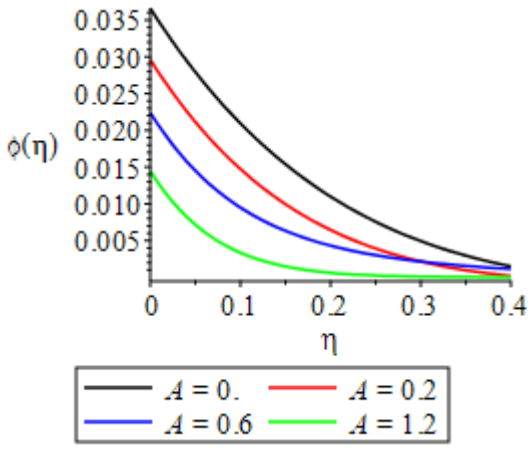

Figure 18: Effect of unsteadiness parameter on Concentration Distributions

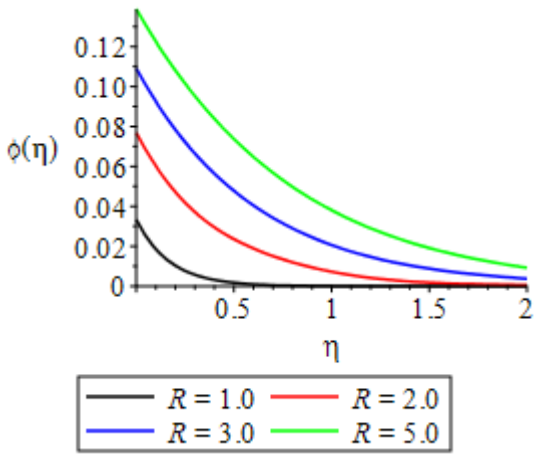

Figure 19: Effect of Radiation parameter on Concentration Distributions

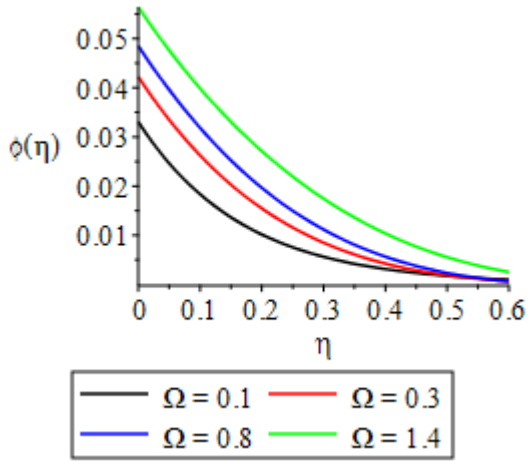

Figure 20: Effect of thermophoretic diffusion parameter on Concentration Distributions

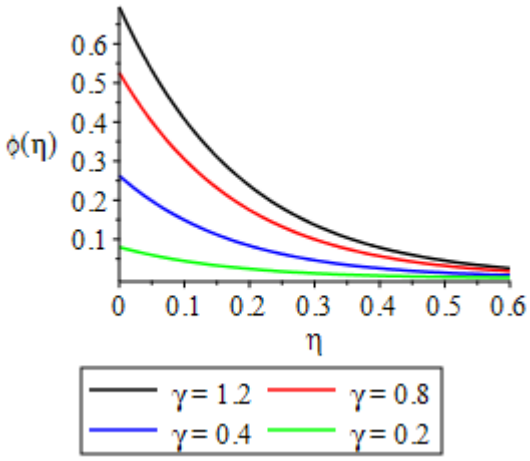

Figure 21: Effect of concentration slip on Concentration Distributions

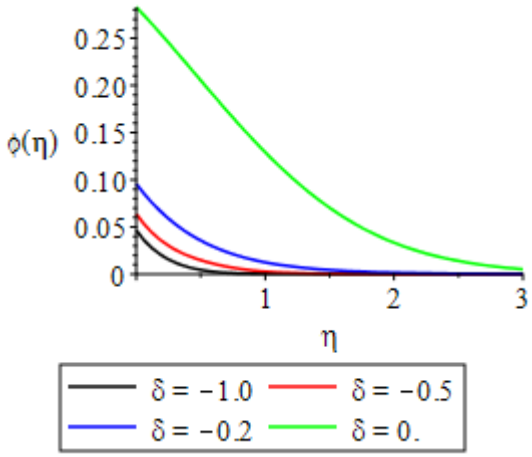

Figure 22: Effect of reactivity parameter on Concentration Distributions

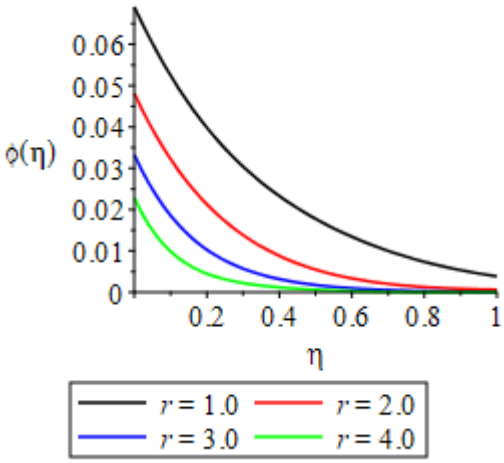

Figure 23: Effect of reaction order on Concentration Distributions

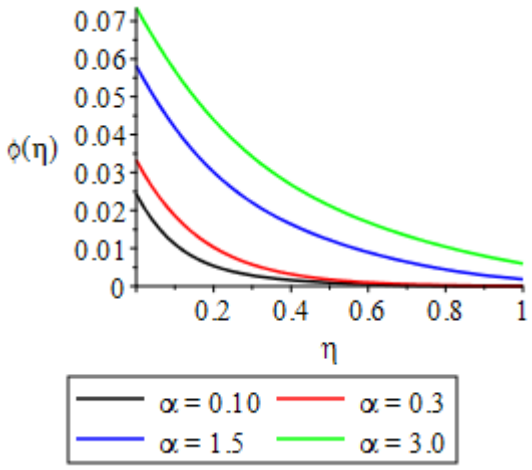

Figure 24: Effect of variable thermal conductivity on Concentration Distributions

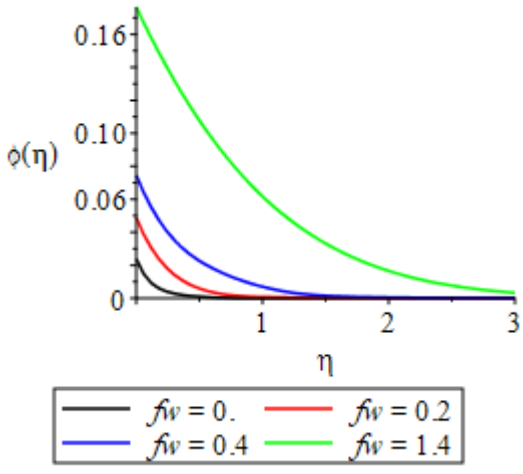

Figure 25: Effect of suction parameter on Concentration Distributions

D. Wall Rate Transfer

The effect of the flow governing parameters on the wall rate transfer skin friction, Sherwood number and Nusselt number is displayed in Table 1. From this table, it is evidently clear that $A, Ec, \beta, \Omega, Grt, \delta, \gamma, Bi, Nt$ and Pr all enhances the skin friction while $Fs, B^*, R, Grc, Ha, \alpha, Nb, fw$ and r decline the strenght of skin friction. In the same analysis, $A, Ec, Pr, \alpha, Sc, Bi, Nt$ and r improves the strenght of Sherwood number conversely, $Grt, Ha, \delta, fw, Fs, B^*$ and Ω decline Sherwood number. So also, we discovered that for Nusselt number, $A, Ec, Sc, \delta, \gamma, Bi, r, Nt$ and Pr increases the value of Nusselt number while $Grt, Ha, R, \alpha, Nb, \Omega$ and fw.

V. CONCLUSION

The unsteady heat and mass transfer in MHD flow of Nano-fluid with buoyancy and variable thermal conductivity has not been adequately reported. Hence in this report, we have considered the aforementioned with particular references to velocity, thermal and chemical species slips. From the discussion above, the following conclusion were drawn

- increase in thermal buoyancy, unsteadiness parameter and suction parameter are seen to increase velocity distributions.
- continuous increments in thermal buoyancy, unsteadiness parameter and suction parameter leads to emergence of maximum velocity close to the surface.
- Hartman number, velocity factor, suction velocity, variable thermal conductivity, radiation parameter reduces the velocity boundary layer,
- temperature boundary layer is enhanced with increase in unsteadiness parameter, Brownian motion parameter and Eckert number while
- radiation, thermal conductivity, Hartmann number and suction decline the temperature.
- It was also discovered that unsteadiness parameter, concentration slip factor, reaction order declines the concentration boundary layer,
- in the same vein, radiation, thermophoretic diffusion parameter, reactivity parameter, thermal conductivity and suction enhances species concentration.

TABLE II: NOMENCLATURE

x, y	flow axes	Greek Symbol	
u, v	Velocity component along x and y-axis ($\mathrm{m\,s^{-2}}$)	ρ_{nf}	Nano-fluid density (kgm^{-3})
T	Temperature field (K)	σ	Electrical conductivity (Sm^{-1})
C	Species concentration field	μ	Fluid viscosity (m^2s^{-1})
g	gravitational acceleration ($\mathrm{m\,s^{-2}}$)	γ	Chemical species slip factor
B_0	Magnetic field of uniform strength	β	Viscoelastic parameter
T_w	surface temperature (K)	Dimensionless group	
Bi	Convective surface heat transfer	θ	dimensionless temperature (K)
Ms	Velocity slip factor	ϕ	dimensionless concentration
T_∞	ambient temperature (K)	Grc	Grashof number
β_t	Volumetric coefficient of thermal expansion	Ω	Thermophoretic diffusion coefficient
C_w	surface concentration	N	buoyancy ratio
C_∞	ambient concentration	Nu	Nusselt number
f_w	Suction velocity	Sh	Sherwood number
β_c	Volumetric coefficient of mass expansion	δ	Chemical reaction parameter
k_T	thermal conductivity ($Wm^{-1}K^{-1}$)	R	radiation parameter
c_p	specific heat capacity at constant pressure ($\mathrm{J\,kg^{-1}K}$)	β	Viscoelastic parameter
D_m	Molecular diffusivity	Ha	Hartmann number

D_T	Thermophoretic Diffusion Coefficient	Pr	Prandtl number
U_∞	ambient velocity	Sc	Schmidt number
A^*, B^*	Space heat source/sink parameter k^{-1}	Ec	Eckert number
k_r	Binary chemical reaction parameter		Subscript
R_G	Universal gas constant	∞	ambient condition
Ha	Hartmann number	w	wall condition
Ea	Activation Energy	$0 < \epsilon \ll 1$	

Authour contribution: All authours contributed equally

Conflict of interest: The authours declare that there is no conflict of interest.

Acknowledgements: The authors would like to appreciate and thank Covenant University management for providing the enabling environment, research facilities. Also, we thank the anonymous referees for their useful suggestions that leads to improvement of the result.

REFERENCES

[1]. S.U.S. Choi, J.A. Eastman, Enhancing Thermal Conductivity of Fluids With Nanoparticles, 231, ASME Publications-Fed, (1995) 99–106.

[2]. J. Buongiorno, Convective transport in nanofluids, J. Heat Transf. 128 (2006) 240–250.

[3]. A.K. Pandey, M. Kumar, Boundary layer flow and heat transfer analysis on Cu-water nanofluid flow over a stretching cylinder with slip, Alex. Eng. J. 56 (2017) 671–677.

[4]. F. Ali, I. Khan, S. Shafie, N. Musthapa, Heat and mass transfer with free convection MHD flow past a vertical plate embedded in a porous medium, Math. Probl. Eng. 2013 (2013) 1–13.

[5]. S. Ahmed, A. Batin, A.J. Chamkha, Numerical/laplace transform analysis for MHD radiating heat/mass transport in a Darcian porous regime bounded by an oscillating vertical surface, Alex. Eng. J. 54 (2015) 45–54.

[6]. R. Muhammad, M.I. Khan, N.B. Khan, M. Jameel, Magnetohydrodynamics (MHD) radiated nanomaterial viscous material flow by a curved surface with second order slip and entropy generation, Comput. Methods Programs Biomed. 189 (2020) 105294.

[7]. R. Muhammad, M.I. Khan, M. Jameel, N.B. Khan, Fully developed Darcy-Forchheimer mixed convective flow over a curved surface with activation energy and entropy generation, Comput. Methods Programs Biomed. 188 (2020) 105298.

[8]. Paolo Di Sia. Mathematics and Physics for Nanotechnology: Technical Tools and Modelling. Taylor and Francis, Pan Stanford Publishing Pte. Ltd. Penthouse Level, Suntec Tower 3 8 Temasek Boulevard Singapore, (2019): 038988 DOI: 10.1201/9780429027758

[9]. Di Sia, Paolo, Present and future of nanotechnologies: peculiarities, Phenomenology, Theoretical Modelling, Perspectives, Rev. Theor. Sci., 2(2), 146 (2014).

[10]. S. Suresh, K.P. Venkitaraj, P. Selvakumar, M. Chandrasekar, Synthesis of Al2O3–Cu/water hybrid nanofluids using two step method and its thermo physical properties, Colloid Surf. A Physicochem. Eng. Asp. 388 (1–3) (2011) 41–48.

[11]. D. Mansoury, F.I. Doshmanziari, S. Rezaie, M.M. Rashidi, Effect of Al2O3/water nanofluid on performance of parallel flow heat exchangers, J. Therm. Anal. Calorim. 135 (1) (2019) 625–643.

[12]. Y. Ma, R. Mohebbi, M.M. Rashidi, O. Manca, Z. Yang, Numerical investigation of MHD effects on nanofluid heat transfer in a baffled U-shaped enclosure using lattice Boltzmann method, J. Therm. Anal. Calorim. 135 (6) (2019) 3197–3213.

[13]. S. Jana, A. Salehi-Khojin, W.H. Zhong, Enhancement of fluid thermal conductivity by the addition of single and hybrid nanoadditives, Thermochim. Acta 462 (1–2) (2007) 45–55.

[14]. J. Sarkar, P. Ghosh, A. Adil, A review on hybrid nanofluids: recent research, development and applications, Renew. Sust. Energ. Rev. 43 (2015) 164–177.

[15]. N.A. Sidik, I.M. Adamu, M.M. Jamil, G.H. Kefayati, R. Mamat, G. Najafi, Recent progress on hybrid nanofluids in heat transfer applications: a comprehensive review, Int. Comm. Heat Mass Transf. 78 (2016) 68–79.

[16]. S. Akilu, K.V. Sharma, A.T. Baheta, R. Mamat, A review of thermophysical properties of water based composite nanofluids, Renew. Sust. Energ. Rev. 66 (2016) 654–678.

[17]. J.R. Babu, K.K. Kumar, S.S. Rao, State-of-art review on hybrid nanofluids, Renew. Sust. Energ. Rev. 77 (2017) 551–565.

[18]. L.S. Sundar, K.V. Sharma, M.K. Singh, A.C. Sousa, Hybrid nanofluids preparation, thermal properties, heat transfer and friction factor–a review, Renew. Sust. Energ. Rev. 68 (2017) 185–198.

[19]. K.Y. Leong, K.K. Ahmad, H.C. Ong, M.J. Ghazali, A. Baharum, Synthesis and thermal conductivity characteristic of hybrid nanofluids–a review, Renew. Sust. Energ. Rev. 75 (2017) 868–878.

[20]. G. Huminic, A. Huminic, Hybrid nanofluids for heat transfer applications–a state-of-the-art review, Int. J. Heat Mass Transf. 125 (2018) 82–103.

[21]. M.U. Sajid, H.M. Ali, Thermal conductivity of hybrid nanofluids: a critical review, Int. J. Heat Mass Transf. 126 (2018) 211–234.

[22]. M. Ghalambaz, S.A. Mehryan, A. Hajjar, A. Veisimoradi, Unsteady natural convection flow of a suspension comprising Nano-Encapsulated Phase Change Materials (NEPCMs) in a porous medium, Adv. Powder Tech. (2019), https://doi.org/10.1016/j.apt.2019.12.010.

[23]. M. Ghalambaz, A.J. Chamkha, D. Wen, Natural convective flow and heat transfer of nano-encapsulated phase change materials (NEPCMs) in a cavity, Int. J. Heat Mass Transf. 138 (2019) 738–749.

[24]. M. Ghalambaz, T. Gros an, I. Pop, Mixed convection boundary layer flow and heat transfer over a vertical plate embedded in a porous medium filled with a suspension of nano-encapsulated phase change materials, J. Mol. Liq. 293 (2019) 111432.

[25]. A. Hajjar, S.A. Mehryan, M. Ghalambaz, Time periodic natural convection heat transfer in a nano-encapsulated phase-change suspension, Int. J. Mech. Sci. 166 (2020) 105243.

[26]. A.J. Chamkha, I.V. Miroshnichenko, M.A. Sheremet, Numerical analysis of unsteady conjugate natural convection of hybrid water-based nanofluid in a semicircular cavity, J. Therm. Sci. Eng. Appl. 9 (4) (2017) 041004.

[27]. M. Ghalambaz, M.A. Sheremet, S.A. Mehryan, F.M. Kashkooli, I. Pop, Local thermal non-equilibrium analysis of conjugate free convection within a porous enclosure occupied with Ag–MgO hybrid nanofluid, J. Therm. Anal. Calorim. 135 (2) (2019) 1381–1398.

[28]. M.A. Sheremet, D.S. Cimpean, I. Pop, Thermogravitational convection of hybrid nanofluid in a porous chamber with a central heat-conducting body, Symmetry 12 (4) (2020) 593.

[29]. Arunachalam, M. and N.R. Rajappa. Forced convection in liquid metals with variable thermal conductivity and capacity. Acta Mechanica 31, (1978) 25-31.

[30]. Chaim, T.C. Heat transfer in a fluid with variable thermal conductivity over stretching sheet. Acta Mechanica 129, (1998). 63-72